Key Points:
- We invert for 2-D flow velocities in Korff Ice Rise, West Antarctica, from radar data and simulate isochrone evolution
- Matching simulated and observed isochrones, we estimate that divide flow began 2.5 (1.8-2.9) kyr B.P. in this location
- This potentially dates a regional ice-flow reorganization, and our data are consistent with flow being slow before and stable after this time

Supporting Information:
- Supporting Information S1

Correspondence to:
J. Kingslake,
j.kingslake@columbia.edu

Ice-flow reorganization in West Antarctica 2.5 kyr ago dated using radar-derived englacial flow velocities

Jonathan Kingslake[1,2], Carlos Martín[1], Robert J. Arthern[1], Hugh F. J. Corr[1], and Edward C. King[1]

[1]Lamont-Doherty Earth Observatory, Palisades, New York, USA, [2]British Antarctic Survey, Natural Environmental Research Council, Cambridge, UK

Abstract We date a recent ice-flow reorganization of an ice divide in the Weddell Sea Sector, West Antarctica, using a novel combination of inverse methods and ice-penetrating radars. We invert for two-dimensional ice flow within an ice divide from data collected with a phase-sensitive ice-penetrating radar while accounting for the effect of firn on radar propagation and ice flow. By comparing isochronal layers simulated using radar-derived flow velocities with internal layers observed with an impulse radar, we show that the divide's internal structure is not in a steady state but underwent a disturbance, potentially implying a regional ice-flow reorganization, 2.5 (1.8–2.9) kyr B.P. Our data are consistent with slow ice flow in this location before the reorganization and the ice divide subsequently remaining stationary. These findings increase our knowledge of the glacial history of a region that lacks dated constraints on late-Holocene ice-sheet retreat and provides a key target for models that reconstruct and predict ice-sheet behavior.

1. Introduction

The West Antarctic Ice Sheet is losing mass and contributing to sea-level rise [*Vaughan et al.*, 2013]. To improve predictions of future ice mass loss, we must determine how ice sheets retreat over time scales longer than the decades elapsed since the beginning of the satellite era. This is needed to test predictive ice-sheet models and place observations of contemporary change in the context of longer-term changes [e.g., *Bentley et al.*, 2014; *DeConto and Pollard*, 2016].

The largest changes in Antarctic ice-sheet extent since the Last Glacial Maximum (LGM) (≈26 to 19 kyr B.P.) [*Clark et al.*, 2009] have occurred in the Weddell and Ross Seas [e.g., *Bentley et al.*, 2010; *Golledge et al.*, 2012; *Whitehouse et al.*, 2012; *Anderson et al.*, 2014; *Hillenbrand et al.*, 2014]. In both regions deglacial ages from marine radiocarbon and cosmogenic exposure dating [e.g., *Conway et al.*, 1999, 2002; *Bentley et al.*, 2010; *Anderson et al.*, 2014; *Fogwill et al.*, 2014], as well as observations of glacio-isostatic adjustment [*Bradley et al.*, 2015], ice surface lineations [e.g., *Fahnestock et al.*, 2000; *Hulbe and Fahnestock*, 2007; *Siegert et al.*, 2013], and ice-sheet internal structure [e.g., *Conway et al.*, 1999; *Catania et al.*, 2012; *Siegert et al.*, 2013; *Bingham et al.*, 2015; *Winter et al.*, 2015] indicate ice-sheet retreat since the LGM and flow reorganization during the last few thousand years.

The details of these ice-flow changes are poorly constrained. For example, geological evidence from the Weddell Sea Sector indicates that the grounding line (the boundary between floating and grounded ice; Figure 1) of the ice sheet was located hundreds of kilometers seaward of its current position during the LGM [*Larter et al.*, 2012; *Hillenbrand et al.*, 2014], but the style and speed of its subsequent landward migration (Figure 1) are unknown [*Hillenbrand et al.*, 2014]. Because this region is thought to be susceptible to future retreat [e.g., *Ross et al.*, 2012; *Wright and ohters*, 2014; *Thoma et al.*, 2015] and ice-sheet reconstructions are used to tune ice-sheet models [e.g., *DeConto and Pollard*, 2016], this lack of knowledge of past flow conditions directly impacts our ability to predict future ice-sheet behavior, increasing the bounds of uncertainty on sea-level predictions.

In areas like the central Weddell Sea Sector, where a lack of accessible deglaciated surfaces makes techniques like marine radiocarbon and cosmogenic exposure dating difficult, a glacio-geophysical technique called Raymond Effect Dating (RED) can be applied at ice divides to constrain ice-sheet flow history [*Conway et al.*, 1999; *Martín et al.*, 2006]. The technique exploits a nonlinear ice-flow phenomenon called the Raymond Effect. Low deviatoric stresses near the bed beneath ice divides create a deep area of relatively stiff ice
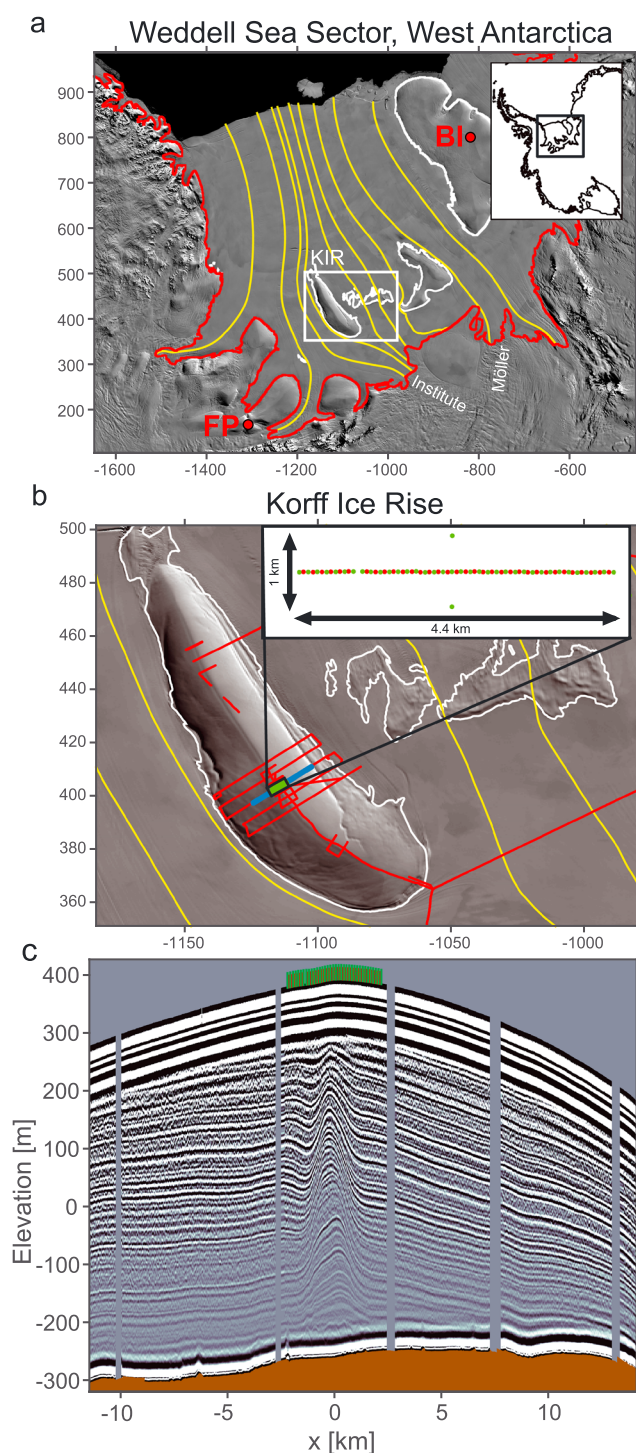
Figure 1. Field site and impulse radargram. (a) The Weddell Sea Sector. Korff Ice Rise (KIR), Institute and Möller Ice Streams, and Fletcher Promontory (FP) and Berkner Island (BI) ice core sites are labeled. White box shows area enlarged in Figure 1b, and inset shows location in West Antarctica. (b) Korff Ice Rise. The radar line producing the radargram in Figure 1c (blue). All other radar lines in the region (red). Inset shows the location of (red) pRES and (green) GPS measurements. Figures 1a and 1b use polar stereographic projection (latitude of true scale 71°S) and imagery from *Haran et al.* [2005] (axes in km). Yellow curves are streamlines computed from satellite-derived velocities [*Rignot et al.*, 2011]. Main ice-sheet grounding line (red) and other grounding lines (white) from *Rignot et al.* [2011]. Impulse radargram crossing the KIR divide with GPS (green) and pRES (red) stakes shown at the surface (Figure 1c). To aid visualization, the data are unmigrated, but layers are picked from migrated data (supporting information). Vertical gray bars indicate regions with no data. Note that within ≈100 m of the surface the airwave obscures internal layers.

[*Raymond*, 1983; *Conway et al.*, 1999; *Martín et al.*, 2006; *Gillet-Chaulet et al.*, 2011; *Matsuoka et al.*, 2015]. The resulting slow vertical flow beneath the divide compared to the flanks causes internal ice layers, assumed to be isochrones, to form anticlinal "Raymond arches," which grow over time beneath ice divides [e.g., *Conway et al.*, 1999; *Vaughan et al.*, 1999; *Nereson and Raymond*, 2001; *Pettit et al.*, 2003; *Pettit and Waddington*, 2003; *Martín et al.*, 2006; *Kingslake et al.*, 2014; *Drews et al.*, 2015]. By modeling or measuring the flow of ice within an ice divide, Raymond arches can be simulated and matched to radar-detected arches in order to estimate when the ice divide first formed in its current location [e.g., *Conway et al.*, 1999]. As ice-divide location depends on ice flow on either side of the divide, this date is interpreted as the last time ice flow in the region underwent reorganization, possibly associated with the grounding line of the main ice sheet migrating through the region [*Conway et al.*, 1999; *Martín et al.*, 2006; *Drews et al.*, 2015; *Matsuoka et al.*, 2015].

Previous applications of RED [e.g., *Conway et al.*, 1999; *Martín et al.*, 2006; *Drews et al.*, 2015] have successfully used ice-flow models to simulate ice flow and Raymond arch growth, providing unique constraints on ice-flow histories in regions where other techniques are impossible. However, these constraints come with significant uncertainty associated with ice-flow parameters, used by ice-flow models, that are poorly constrained at ice divides [*Drews et al.*, 2015]. Specifically, radar observations from Greenland [*Gillet-Chaulet et al.*, 2011] and Antarctica [*Kingslake et al.*, 2014] suggest that ice-flow parameterizations underestimate the nonlinearity of englacial vertical velocity profiles at ice divides when these parameterizations use common values for ice-flow parameters.

Here we apply RED at an ice divide on Korff Ice Rise (KIR), SW Weddell Sea. We avoid some of the uncertainty associated with model-based RED by inverting for two-dimensional (2-D) ice-flow fields within the ice divide from data collected with a phase-sensitive radar. We do not assume a specific model for the viscosity of ice, but our inversion is not free from ice-flow assumptions, and we assess the validity of these assumptions and the accuracy of the flow fields using two independent data sets. Comparisons between Raymond arches simulated using radar-derived flow fields and Raymond arches observed with an impulse radar system indicate that the most recent reorganization in the flow of KIR occurred 2.5 (1.8–2.9) kyr B.P. We discuss sources of uncertainty, the limitations of our new inverse method, and future improvements to our inverse method, before considering possible causes of this flow reorganization.

2. Methods

During two field seasons (2013/2014 and 2014/2015) we deployed two ground-based ice-penetrating radar systems along a survey line centered on and perpendicular to the ice divide that bisects KIR, a slow-moving (less than 10 m yr^{-1} at the surface) grounded region surrounded by the Ronne Ice Shelf, West Antarctica (Figure 1). Along our survey line ice is approximately 600 m thick, grounded 250 m below sea level and cold based, as indicated by seismic reflection data (A. Smith, personal communication, 2015). We used a 4 MHz impulse ice-penetrating radar [*Hindmarsh et al.*, 2011] to map internal layer structure (Figures 1c and the supporting information) and at 35 equally spaced stakes extending ±2.2 km from the divide we deployed a phase-sensitive step-frequency radar (pRES) in both seasons. Data collected with pRES are used to compute the two-way travel time of radio waves to internal reflectors within the ice and the ice-sheet base. Also, by comparing data collected in each season, we compute how the phase of the radar return from each reflector changed relative to a specific bright reflector during the intervening period (approximately 1 year; supporting information) [*Corr et al.*, 2002; *Jenkins et al.*, 2006; *Gillet-Chaulet et al.*, 2011; *Kingslake et al.*, 2014].

Because internal reflectors move with the ice as it flows, these data contain information about englacial flow. We developed a method (following *Chartrand* [2011] and *Petra and Stadler* [2011]) to invert for horizontal and vertical flow fields from the pRES data, simultaneously deriving a density field. Density is important because it affects the propagation of radio waves [*Kovacs et al.*, 1995] and the calculation of horizontal strain rates from the vertical velocities. We assume vertically uniform horizontal strain rates in the upper 200 m in the flanks when inverting for density (section 4.5 in supporting information; near the divide the Raymond Effect invalidates this assumption) [*Dansgaard and Johnsen*, 1969]. We also assume that the density profile is steady state, uniform horizontally and approaches the density of ice exponentially with depth (supporting information). We also assume that the ice is stretching horizontally and that there is no basal sliding. The method takes account of the separation of the pRES antennas (7 m) and the refraction of the radar signal as it travels through the firn [*Arthern et al.*, 2013]. Horizontal strain rates are integrated from the divide summit, located using surface
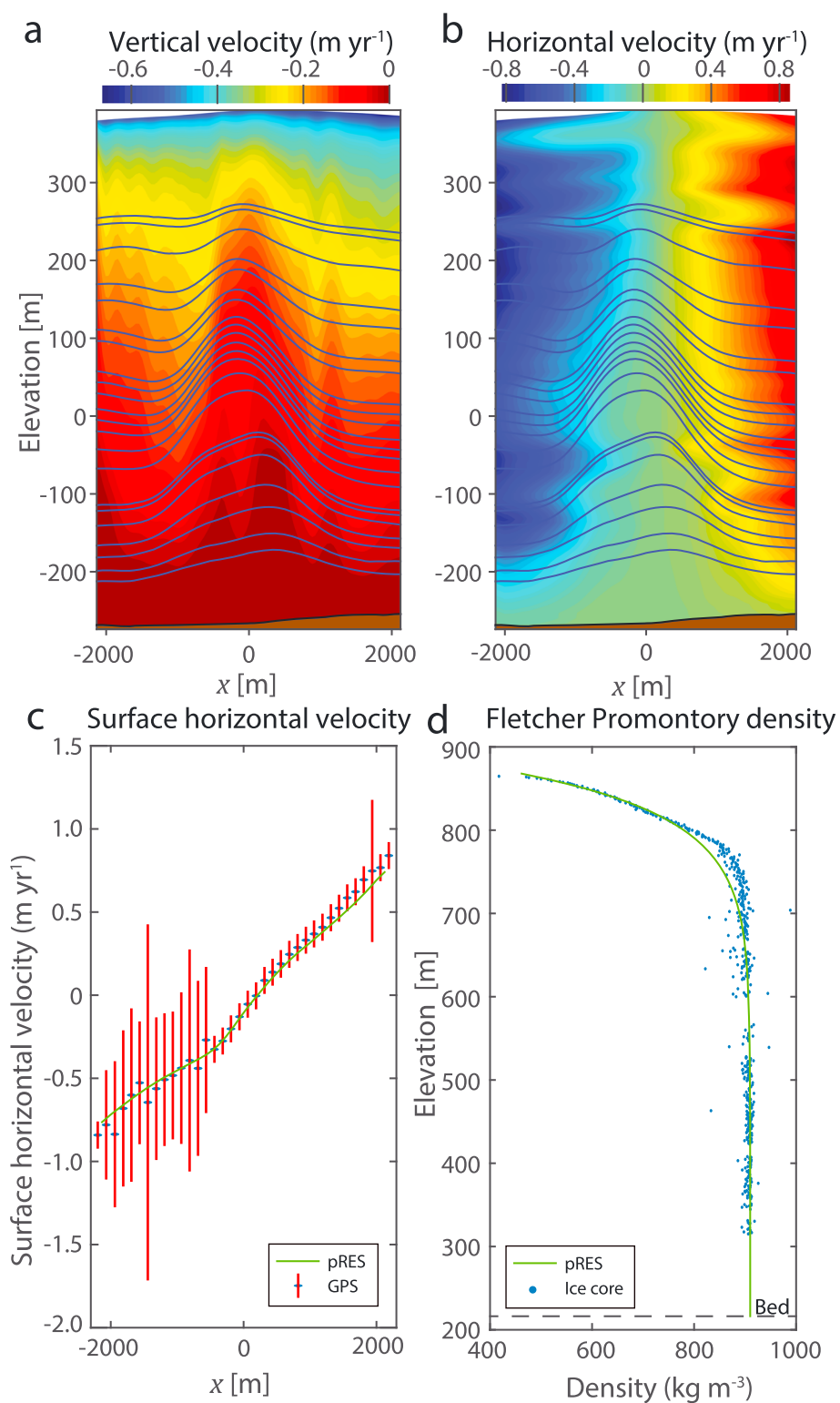
Figure 2. Inverted ice flow and density fields. pRES-derived (a) vertical and (b) horizontal ice velocities plotted with internal layers picked from impulse radar data (blue). Elevations relative to the WGS84 ellipsoid. (c) Horizontal surface velocities on KIR (blue and red crosses) measured by dual-band GPS, with the height the crosses indicating uncertainties, and (green) inverted from pRES data. Higher uncertainties of GPS measurements where $x \leq -565$ m are due to a power failure of the base GPS station (supporting information). (d) Density profiles from Fletcher Promontory (blue) measured directly from an ice core and (green) inverted for from pRES data.

elevation data from a Global Positioning Systems (GPS) unit mounted on the impulse radar (supporting information), to compute horizontal velocities. The results are 2-D, mass-conserving, density-corrected fields of horizontal and vertical ice flow (Figure 2a and 2b) and a corresponding vertical density profile.

To assess the accuracy of the flow fields, in both field seasons we conducted two additional surveys: we used dual-band GPS to measure horizontal surface velocities on KIR (Figure 1b and the supporting information) and we deployed pRES on Fletcher Promontory, an ice rise close to KIR (Figure 1a), to compute a density profile using our inverse method at a location where densities have been measured directly from an ice core (Figure 1a) [*Mulvaney et al.*, 2014].

We simulate the transient evolution of internal layers using the inverted ice-flow fields. Layers are initially flat, and at each time step (25 years) their elevations evolve according to the inverted flow fields. This generates an evolving set of simulated Raymond arches. To compare the simulated arches with arches observed with the impulse radar, the amplitudes of each are calculated separately relative to the east and west flanks ($-2.1 \le x \le -1.2$ km and $1.2 \le x \le 2.1$ km) using layer elevations normalized with local ice thickness. We difference each layer's mean normalized elevation in each flank with its maximum normalized elevation [e.g., *Conway et al.*, 1999]. Arch amplitudes are calculated as the product of the normalized elevation differences and the ice thickness at the arch apex. Finally, for each layer a mean arch amplitude is calculated from pairs of amplitudes calculated relative to each flank. When comparing simulated and observed arches, we use the mean arch amplitude and amplitudes measured relative to each flank separately.

3. Results

Figures 2a and 2b plot vertical and horizontal velocity fields obtained from inverting pRES measurements, overlain with internal layers picked from the impulse data (Figure 1c and the supporting information). The anticlines in the vertical velocity contours (Figure 2a) are consequences of the Raymond Effect. After assessing the accuracy of the velocity fields, we will show that the anticlinal Raymond arches observed in the internal layers with the impulse radar (Figures 1c, 2a, and 2b) are the result of the Raymond Effect acting at this location for around 2.5 kyr.

We assess the accuracy of the inverted velocity fields using two independent data sets. Figure 2c plots horizontal surface velocities measured with GPS (supporting information) with horizontal surface velocities extracted from the inverted horizontal velocity field (Figure 2b). While the agreement is excellent, the slight underestimation of horizontal velocities suggests inaccuracy in the inverted density profile, which impacts horizontal surface velocities through the dependence of radar-wave speed on density and the steady-state compaction rate associated with the density profile. This is likely linked to an unphysical feature of the horizontal velocity field, where horizontal velocities increase with depth over a short distance near the surface. This also occurs to a lesser extent deeper in the ice column, where the cause is instrumental noise. As discussed later, additionally constraining our flow fields to obey mechanical ice-flow equations would remove this, but it is beyond our scope, and it is unlikely to significantly affect our key results.

Figure 2d compares a density profile inverted from pRES data collected at the site of the Fletcher Promontory ice core against measured ice-core densities (R. Mulvaney, personal communication, 2015). In the top 60 m of the ice column the match is very close. The mismatch at elevations between 700 m and 800 m is likely to be due to our assumption that the density varies exponentially with depth, while the true vertical density variation may be more complex.

These comparisons between independent data sets indicate that the inverse method computes reasonably accurate flow fields, albeit with some unphysical features in the horizontal flow field related to instrumental noise and the inadequacy of the density parameterization. In particular, the comparisons suggest that uncertainties in the simulation of layer structure will be not be dominated by uncertainty in the flow fields. They also suggest that our assumptions of zero basal sliding, horizontally uniform densities and negligible ice-surface slope are appropriate.

Using our layer-tracking scheme and ice velocities inverted for from pRES data, we evolve layers for 15 kyr. We find that approximately steady-state Raymond arches form beneath the divide. Figure 3a plots these simulated arches over present-day arches observed beneath KIR. Simulated arches form in the same place as present-day arches and have similar widths (≈ 2 km). The simulation also partially captures the asymmetry
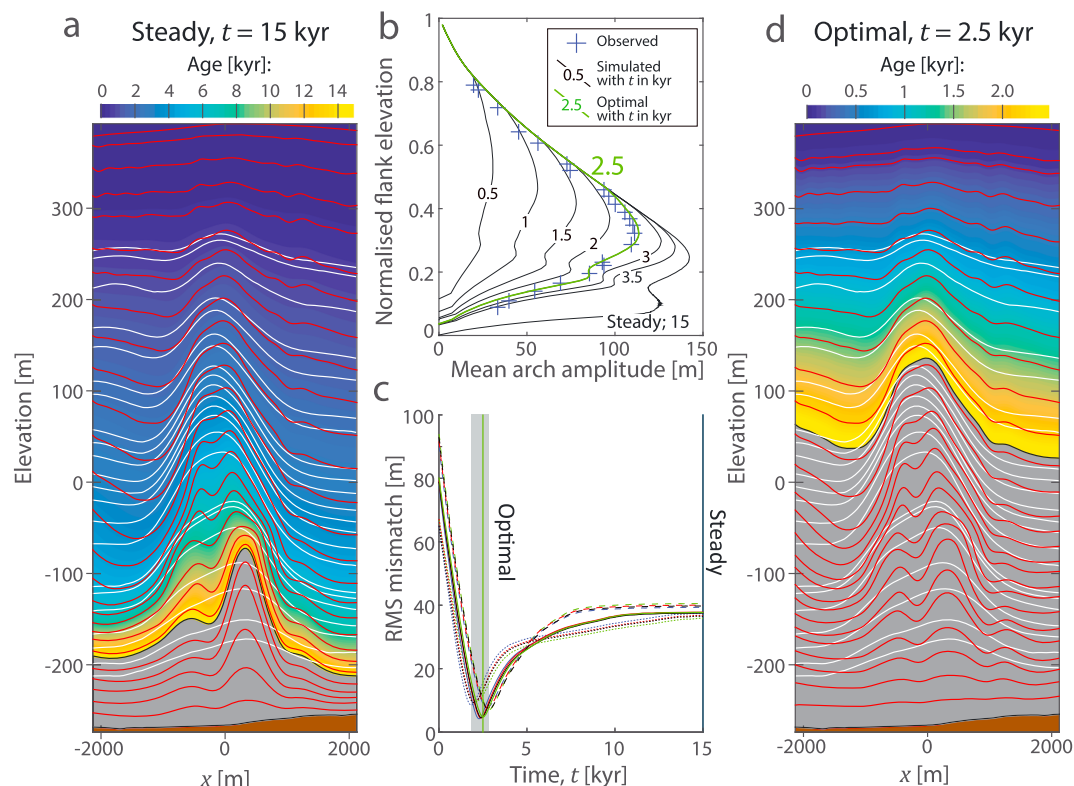
Figure 3. Observed and simulated Raymond arches at Korff Ice Rise. (a) Overlain on the observed arches (white) are steady state simulated arches (red) (t = 15 kyr). The color map shows the corresponding age field; ice present at the start of the simulation is in gray. (b) Simulated and observed arch amplitudes calculated as the mean of the amplitudes measured relative to each flank (−2.1≤x≤ −1.2 km and 1.2≤x≤2.1 km) at eight time slices. (c) Time series of mismatch between simulated and observed arch amplitudes from 12 simulations, each using an alternative arch amplitude calculation. Dashed, dotted, and solid curves, respectively, correspond to arches measured relative to the eastern flank, relative to the western flank, and as the average of the two. Colors correspond to four alternative flank regions (in km): (green) −2.1 to −1.2, 1.2 to 2.1; (red) −1.9 to −1, 1 to 1.9; (black) −1.9 to −1.2, 1 to 2.1; and (blue) −2.1 to −1, 1.9 to 2.1. The gray box shows the range of the 12 optimal matches. (d) Identical to Figure 3a but shows the optimal match at 2.5 kyr from the simulation in Figure 3b.

of the observed layers in the flanks likely to result from an across-divide accumulation gradient [*Nereson and Raymond*, 2001; *Drews et al.*, 2015]. However, the steady-state simulated layers have a prominent central syncline overlain on the Raymond arches, producing so-called "double arches" [e.g., *Martín et al.*, 2009], and they are significantly larger in amplitude than present-day arches (Figure 3b).

This implies that the ice-flow pattern caused by the Raymond Effect has not been in operation for long enough to allow the Raymond arches to reach a steady state within KIR. Alternatively, ice-divide thickening, stochastic divide migration, along-ridge flow or basal sliding could have suppressed Raymond arch growth in KIR and might explain the relatively small observed arches [*Martín et al.*, 2009]. However, thickening would have caused the steady-state simulation to overestimate the elevation of the maximum arch amplitude [*Martín et al.*, 2006]. Instead, the simulation underestimates this elevation (Figure 3b). Stochastic divide migration would have widened the observed arches [*Martín et al.*, 2009], causing the simulation to underestimate arch width. Instead, the width of the two sets of arches are approximately equal (Figure 3a). Negligible along-ridge flow (≈ 0.04 m yr^{-1}; supporting information) was recorded by the surface GPS survey and significant basal sliding is inconsistent with a cold ice-sheet bed, as indicated by seismic surveys.

The best explanation for the mismatch between the amplitudes of the observed arch and those produced in our steady-state simulation is that ice on KIR experienced a recent reorganization in flow that allowed the divide to form in its current location.

To estimate when the flow reorganization occurred, we track the agreement between simulated and observed Raymond arches over time using the root-mean-square (RMS) mismatch between their mean amplitudes,

calculated as the mean of amplitudes measured relative to each flank (Figure 3c). An optimal match (with an RMS residual of 4.7 m) between the simulation and the observations at $t = 2.5$ kyr (Figures 3b and 3c) supplies our best estimate of the time elapsed since the ice divide formed in its current location on KIR. Figures 3b and 3d compare simulated and observed arches at $t = 2.5$ kyr. Notwithstanding the "double arch" structure in the simulation (Figure 3d), which we discuss later, the match is excellent. In particular, the widths of the simulated and observed arches and the elevations at which they attain their maximum amplitudes match closely. This is consistent with negligible thickening, thinning, or migration of the ice divide since it formed 2.5 kyr B.P.

One source of uncertainty in this ice-divide formation date is the choice of where to measure the elevations of layers in the flanks while calculating arch amplitudes. To take account of this uncertainty, we conduct 12 simulations while varying the regions in each flank used to measure arch amplitudes and the flank used in the calculation, i.e., we consider amplitudes calculated (1) relative to the east flank, (2) relative to the west flank, and (3) as the mean of the amplitudes measured relative to each flank. Figure 3c plots time series of the RMS mismatch from all 12 simulations. These yield a range of optimal times between 1.8 kyr and 2.9 kyr, reflecting the fact that the observed arches are more asymmetric than the simulated arches (Figure 3d). The range 1.8–2.9 kyr B.P. represents a range of possible ice-divide formation dates.

Our assumption that ice flow within the divide has not changed since divide flow began also introduces uncertainty. Although our findings are consistent with steady flow, this uncertainty probably dominates uncertainty associated with observations of arch amplitudes (approximately ±5 m; supporting information) and ice velocities (comparison between GPS-derived and inverted surface velocities indicates that these are small; Figure 2c). Past ice flow may have varied due to evolving accumulation rates or ice rheology, the latter caused by ice fabric or temperature evolution. Ice-core data covering the last 1 kyr from Berkner Island (Figure 1a) indicate approximately constant accumulation rates over this period [*Mulvaney et al.*, 2002], although previously higher accumulation would cause us to overestimate the age of the Raymond arches and previously lower accumulation would cause us to underestimate their age. Ice-fabric evolution enhances the Raymond Effect over time [e.g., *Pettit et al.*, 2007; *Martín et al.*, 2009, 2014], so the double-arch structure in the vertical velocity field (Figure 2a), which is consistent with ice-fabric development [*Martín et al.*, 2009], may indicate that the Raymond Effect was weaker in the past, causing us to underestimate the age of the arches.

We prescribed the initial isochrones to be flat in all simulations. If the ice was fast moving before the divide formed, layers may have been disturbed and undulating [e.g., *Siegert et al.*, 2013; *Bingham et al.*, 2015]. Experimentation with simulations initialized with layer undulations show that this does not significantly affect our estimation of ice-divide formation time because undulations are quickly reduced in amplitude by horizontal spreading in the vicinity of the divide.

4. Discussion

For the first time phase-sensitive radar data has been inverted for two-dimensional vertical and horizontal englacial flow fields and densities. This new capability has the potential to transform the way we observe ice sheets and ice shelves. In addition to its application here to constrain ice-flow history, it can be used to plan and date ice cores [e.g., *Martín et al.*, 2015] and improve ice-rheology parameterizations. Similar techniques could be applied in other glaciological settings where understanding englacial ice flow is important, for example, to improve measurements of subshelf melting [*Nicholls et al.*, 2015] and to examine the effect of tides on ice-shelf and ice-stream flow.

Several improvements to our inverse method are possible. We use regularization to constrain our velocity fields to vary smoothly (supporting information), in recognition that our data contain high-frequency noise. We selected a level of regularization to compromise between conforming to the data and "smoothing out" noise (supporting information). To make this choice more rigorous, future work could take a Bayesian statistical approach [e.g., *Arthern*, 2015].

Our inverted velocity fields are constrained to conserve mass. It is possible to additionally constrain them to conserve momentum with the compressible Stokes equations [e.g., *Zwinger et al.*, 2007]. This advance would improve the accuracy of the derived velocity fields by removing the unphysical vertical variability in horizontal velocities. Because horizontal flow only affects the width of simulated arches and vertical flow fields that obey mass and momentum conservation will be constrained by radar data, this advance is unlikely to significantly adjust our key results but it could provide information about ice rheology [*Gillet-Chaulet et al.*, 2011].

Our treatment of uncertainties in the date of ice-divide formation on KIR is simplified. Through comparison with independent, but spatially limited, measurements of ice flow and density, we argue that uncertainty in the date of ice-divide formation associated with the flow-field inversion is dominated by uncertainty associated with assuming constant ice flow during simulations. We discussed what could have caused deviations from constant flow and how these would impact our results, and we estimated uncertainty by comparing our simulated Raymond arches to arches measured in the observations relative to each flank individually. This provided a range ice-divide formation dates (1.8–2.9 kyr B.P.) because observed layer structure is more asymmetric than simulated layer structure. Future work could propagate uncertainties in the radar data through the inversion methodology using a Bayesian or Monte Carlo approach to quantify their impact on our estimated date range and the derived density profile.

Other simplifications that could be removed in future work include our prescription of strain rate boundary conditions (supporting information) and our assumptions of small ice-sheet surface and bed slopes, positive horizontal strain rates and steady state, horizontally uniform densities that are known to vary significantly across some ice divides [*Drews et al.*, 2016].

5. Implications and Outlook

We have shown that the isochrone structure beneath the ice divide on KIR is not in a steady state. Instead, the divide formed in its present location 2.5 (1.8–2.9) kyr B.P. and its isochrone structure continues to respond to this flow change. Less clear is the flow regime in this location prior to this time and the cause of divide formation. Did ice in this location flow from a local independent flow center as it does today? And, if not, was ice fast flowing in this location at this time? Alternatively, was ice in this location previously afloat and did the divide form as the ice shelf grounded on the seafloor?

If ice was formerly fast flowing in this location, we would expect to see evidence of large undulations in internal layers or basal crevasses usually associated with fast flow [e.g., *Siegert et al.*, 2013]. Similarly, basal crevassing or rifting could be produced by the grounding of an ice shelf on the seafloor. Instead, layers in ice that, according to our optimal simulation (Figure 3d), was present during divide formation are largely flat and conformable, and show no sign of relic basal crevasses the our survey on KIR (Figure 1b). Therefore, we suggest that ice in this location was grounded and slow flowing prior to divide formation.

We did not observe relic Raymond arches anywhere in our impulse radar survey of KIR (Figure 1b), which would indicate a past divide position [e.g., *Drews et al.*, 2015]. This suggests that ice did not flow from an independent flow center. However, if the ice divide was continuously migrating prior to stabilization 2.5 kyr B.P., Raymond arches could have been preventing from forming. Or the relic features could have been subsequently removed by ice flow over the grounding line and out of the surveyed region. In either case, we would see no evidence of the previous local flow center.

The controls on divide formation are poorly understood [*Matsuoka et al.*, 2015]. We do not know if the divide formed in its current position due to large changes in surface mass balance patterns or a change in regional ice flow. With no evidence for a surface mass balance change, it is worth asking what regional flow changes could have allowed the divide to form 2.5 (1.8–2.9) kyr B.P.

At the LGM the main ice sheet's grounding line was positioned to the north of KIR [e.g., *Bentley et al.*, 2010; *Golledge et al.*, 2012; *Hillenbrand et al.*, 2014]. We hypothesize that its subsequent migration past KIR to its current position (in red in Figure 1a) could have altered ice flow on KIR sufficiently to explain our findings. Prior to this the divide on KIR may have been in a different location or orientation, due to different ice fluxes in the flanks, or the main ice sheet may have overridden the area entirely and prevented ice-divide formation [e.g., *Matsuoka et al.*, 2015].

Alternatively, 2.5 (1.8–2.9) kyr B.P. may correspond to the cessation of regional flow reorganization, for example, as the main ice-sheet grounding line arrived in its current position (Figure 1a). This is consistent with our hypothesis that the ice divide's position and thickness have not changed since its formation, despite recent asymmetric changes in the flow of the adjacent ice shelf [*Scambos et al.*, 2004].

Our observations can potentially be reconciled with hypothesized middle-to-late Holocene ice-shelf grounding and grounding-line advance in the region [*Siegert et al.*, 2013; *Bradley et al.*, 2015]. The ice shelf could have grounded in the location of KIR but continued to undergo persistent flow disturbance,

preventing Raymond-arch formation until around 2.5 kyr B.P. when regional ice flow stabilized. Grounding of the ice-shelf on the seabed would produce significant backstress on the upstream ice streams, potentially causing large-scale readvance [*Matsuoka et al.*, 2015].

In summary, we do not know if an independent flow center existed before 2.5 kyr B.P. on KIR, but our impulse radar data suggest that ice was grounded and slow flowing for long enough prior to divide formation for evidence of fast flow or ice-shelf grounding to have been advected away. The divide could have formed due to the grounding line of the main ice sheet retreating past this location or as regional flow reorganization ceased, perhaps after a grounding of the ice shelf and grounding line advance. Regional ice-flow modeling [e.g., *Fogwill et al.*, 2014; *Wright and ohters*, 2014; *Thoma et al.*, 2015] and geophysical surveys of other ice rises in the region could be used to test these contrasting ice-flow histories and investigate the connection between the reorganization we have dated and the undated switches in flow of the Institute and Möller Ice Streams (Figure 1) inferred from airborne radar data [*Siegert et al.*, 2013; *Bingham et al.*, 2015; *Winter et al.*, 2015].

This work transforms our ability to measure ice flow and constrain ice-sheet history at ice divides. Our improved Raymond Effect dating technique can be applied at ice divides across Antarctica to fill wide gaps in the glacial-geological record that exist where other techniques are impossible due to a lack of exposed geological surfaces [e.g., *Bentley et al.*, 2010]. With ice-sheet models increasingly relying on past ice-sheet configurations to tune poorly constrained parameterizations [e.g., *DeConto and Pollard*, 2016], filling these gaps in the paleoice-sheet record will decrease uncertainty in predictions of sea-level rise.

References

Anderson, J. B., et al. (2014), Ross Sea paleo-ice sheet drainage and deglacial history during and since the LGM, *Quat. Sci. Rev.*, *100*, 31–54.

Arthern, R. J. (2015), Exploring the use of transformation group priors and the method of maximum relative entropy for bayesian glaciological inversions, *J. Glaciol.*, *61*(229), 947–962.

Arthern, R. J., H. F. J. Corr, F. Gillet-Chaulet, R. L. Hawley, and E. M. Morris (2013), Inversion for the density-depth profile of polar firn using a stepped-frequency radar, *J. Geophys. Res. Earth Surf.*, *118*(3), 1257–1263, doi:10.1002/jgrf.20089.

Bentley, M. J., C. J. Fogwill, A. M. Le Brocq, A. L. Hubbard, D. E. Sugden, T. J. Dunai, and S. P. Freeman (2010), Deglacial history of the West Antarctic Ice Sheet in the Weddell Sea Embayment: Constraints on past ice volume change, *Geology*, *38*(5), 411–414.

Bentley, M. J., et al. (2014), A community-based geological reconstruction of Antarctic Ice Sheet deglaciation since the Last Glacial Maximum, *Quat. Sci. Rev.*, *100*, 1–9.

Bingham, R. G., D. M. Rippin, N. B. Karlsson, H. F. Corr, F. Ferraccioli, T. A. Jordan, A. M. Le Brocq, K. C. Rose, N. Ross, and M. J. Siegert (2015), Ice-flow structure and ice dynamic changes in the Weddell Sea Sector of West Antarctica from radar-imaged internal layering, *J. Geophys. Res. Earth Surf.*, *120*(4), 655–670, doi:10.1002/2014JF003291.

Bradley, S. L., R. C. A. Hindmarsh, P. L. Whitehouse, M. J. Bentley, and M. A. King (2015), Low post-glacial rebound rates in the Weddell Sea due to Late Holocene ice-sheet readvance, *Earth Planet Sc. Lett.*, *413*, 79–89, doi:10.1016/j.epsl.2014.12.039.

Catania, G., C. Hulbe, H. Conway, T. A. Scambos, and C. Raymond (2012), Variability in the mass flux of the Ross ice streams, West Antarctica, over the last millennium, *J. Glaciol.*, *58*(210), 741–752.

Clark, P. U., A. S. Dyke, J. D. Shakun, A. E. Carlson, J. Clark, B. Wohlfarth, J. X. Mitrovica, S. W. Hostetler, and A. M. McCabe (2009), The Last Glacial Maximum, *Science*, *325*(5941), 710–714.

Chartrand, R. (2011), Numerical differentiation of noisy, nonsmooth data, *ISRN Appl. Math.*, *2011*, 1023–1033, doi:10.5402/2011/164564.

Conway, H., B. L. Hall, G. H. Denton, A. M. Gades, and E. D. Waddington (1999), Past and future grounding-line retreat of the West Antarctic Ice Sheet, *Science*, *286*, 280–283.

Conway, H., G. Catania, C. Raymond, A. Gades, T. Scambos, and H. Engelhardt (2002), Switch of flow direction in an Antarctic ice stream, *Nature*, *419*(6906), 465–467.

Corr, H. F. J., A. Jenkins, K. W. Nicholls, and C. S. M. Doake (2002), Precise measurement of changes in ice-shelf thickness by phase-sensitive radar to determine basal melt rates, *Geophys. Res. Lett.*, *29*(8), 1232, doi:10.1029/2001GL014618.

Dansgaard, W., and S. J. Johnsen (1969), A flow model and a time scale for the ice core from Camp Century, Greenland, *J. Glaciol.*, *8*, 215–223.

DeConto, R. M., and D. Pollard (2016), Contribution of Antarctica to past and future sea-level rise, *Nature*, *531*(7596), 591–597.

Drews, R., K. Matsuoka, C. Martín, D. Callens, N. Bergeot, and F. Pattyn (2015), Evolution of Derwael Ice Rise in Dronning Maud Land, Antarctica, over the last millennia, *J. Geophys. Res. Earth Surf.*, *120*(3), 564–579, doi:10.1002/2014JF003246.

Drews, R., J. Brown, K. Matsuoka, E. Witrant, M. Philippe, B. Hubbard, and F. Pattyn (2016), Constraining variable density of ice shelves using wide-angle radar measurements, *Cryosphere*, *10*(2), 811–823.

Fahnestock, M., T. Scambos, R. Bindschadler, and G. Kvaran (2000), A millennium of variable ice flow recorded by the Ross Ice Shelf, Antarctica, *J. Glaciol.*, *46*(155), 652–664.

Fogwill, C., C. Turney, N. Golledge, D. Rood, K. Hippe, L. Wacker, R. Wieler, E. Rainsley, and R. Jones (2014), Drivers of abrupt holocene shifts in West Antarctic ice stream direction determined from combined ice sheet modelling and geologic signatures, *Antarc. Sci.*, *26*(06), 674–686.

Gillet-Chaulet, F., R. C. A. Hindmarsh, H. F. J. Corr, E. C. King, and A. Jenkins (2011), In-situ quantification of ice rheology and direct measurement of the Raymond Effect at Summit, Greenland using a phase-sensitive radar, *J. Geophys. Res.*, *38*, L24503, doi:10.1029/2011GL049843.

Golledge, N. R., C. J. Fogwill, A. N. Mackintosh, and K. M. Buckley (2012), Dynamics of the Last Glacial Maximum Antarctic ice-sheet and its response to ocean forcing, *Proc. Natl. Acad. Sci. U.S.A.*, *109*(40), 16,052–16,056.

Haran, T., J. Bohlander, T. Scambos, T. Painter, and M. Fahnestock (2005), *MODIS Mosaic of Antarctica (MOA) Image Map*, Digital media, Natl. Snow and Ice Data Cent., Boulder, Colo.

Hillenbrand, C.-D. et al. (2014), Reconstruction of changes in the Weddell Sea Sector of the Antarctic Ice Sheet since the Last Glacial Maximum, *Quat. Sci. Rev.*, *100*, 111–136.

Hindmarsh, R. C. A., E. C. King, R. Mulvaney, H. F. J. Corr, G. Hiess, and F. Gillet-Chaulet (2011), Flow at ice-divide triple junctions: 2. Three-dimensional views of isochrone architecture from ice-penetrating radar surveys, *J. Geophys. Res.*, *116*(F15), F02024, doi:10.1029/2009JF001622.

Hulbe, C., and M. Fahnestock (2007), Century-scale discharge stagnation and reactivation of the Ross ice streams, West Antarctica, *J. Geophys. Res.*, *112*, F03S27, doi:10.1029/2006JF000603.

Jenkins, A., H. F. Corr, K. W. Nicholls, C. L. Stewart, and C. S. Doake (2006), Interactions between ice and ocean observed with phase-sensitive radar near an Antarctic ice-shelf grounding line, *J. Glaciol.*, *52*(178), 325–346, doi:10.3189/172756506781828502.

Kingslake, J., R. C. A. Hindmarsh, G. Aðalgeirsdóttir, H. Conway, H. F. J. Corr, F. Gillet-Chaulet, C. Martín, E. C. King, R. Mulvaney, and H. D. Pritchard (2014), Full-depth englacial vertical ice sheet velocities measured using phase-sensitive radar, *J. Geophys. Res. Earth Surf.*, *119*, 2604–2618, doi:10.1002/2014JF003275.

Kovacs, A., A. J. Gow, and R. M. Morey (1995), The in-situ dielectric constant of polar firn revisited, *Cold Reg. Sci. Technol.*, *23*(3), 245–256.

Larter, R. D., A. G. Graham, C.-D. Hillenbrand, J. A. Smith, and J. A. Gales (2012), Late quaternary grounded ice extent in the Filchner Trough, Weddell Sea, Antarctica: New marine geophysical evidence, *Quat. Sci. Rev.*, *53*, 111–122.

Martín, C., R. C. A. Hindmarsh, and F. J. Navarro (2006), Dating ice flow change near the flow divide at Roosevelt Island, Antarctica, by using a thermomechanical model to predict radar stratigraphy, *J. Geophys. Res.*, *111*, F01011, doi:10.1029/2005JF000326.

Martín, C., G. H. Gudmundsson, H. D. Pritchard, and O. Gagliardini (2009), On the effects of anisotropic rheology on ice flow, internal structure, and the age-depth relationship at ice divides, *J. Geophys. Res.*, *114*, F04001, doi:10.1029/2008JF001204.

Martín, C., R. C. A. Hindmarsh, and F. J. Navarro (2009), On the effects of divide migration, along-ridge flow, and basal sliding on isochrones near an ice divide, *J. Geophys. Res.*, *114*, F02006, doi:10.1029/2008JF001025.

Martín, C., G. H. Gudmundsson, H. D. Pritchard, and O. Gagliardini (2009), On the effects of anisotropic rheology on ice flow, internal structure, and the age-depth relationship at ice divides, *J. Geophys. Res.*, *114*, F04001, doi:10.1029/2008JF001204.

Martín, C., G. H. Gudmundsson, and E. C. King (2014), Modelling of Kealey Ice Rise, Antarctica, reveals stable ice-flow conditions in East Ellsworth Land over millennia, *J. Glaciol.*, *60*(219), 139–146.

Martín, C., R. Mulvaney, G. H. Gudmundsson, and H. Corr (2015), Inferring palaeo-accumulation records from ice-core data by an adjoint-based method: Application to James Ross Island's ice core, *Clim. Past.*, *11*(3), 547–557, doi:10.5194/cp-11-547-2015.

Matsuoka, K., et al. (2015), Antarctic ice rises and rumples: Their properties and significance for ice-sheet dynamics and evolution, *Earth, Sci. Rev.*, *150*, 724–745, doi:10.1016/j.earscirev.2015.09.004.

Mulvaney, R., J. Triest, and O. Alemany (2014), The James Ross Island and the fletcher promontory ice-core drilling projects, *Ann. Glaciol*, *55*, 179–188, doi:10.3189/2014AoG68A044.

Mulvaney, R., H. Oerter, D. Peel, W. Graf, C. Arrowsmith, E. Pasteur, B. Knight, G. Littot, and W. Miners (2002), 1000 year ice-core records from Berkner Island, Antarctica, *Ann. Glaciol.*, *35*, 45–51.

Nereson, N. A., and C. F. Raymond (2001), The elevation history of ice streams and the spatial accumulation pattern along the Siple Coast West Antarctica inferred from ground-based radar data from three inter-ice-stream ridges, *J. Glaciol.*, *47*(157), 303–313.

Nicholls, K. W., H. F. Corr, C. L. Stewart, L. B. Lok, P. V. Brennan, and D. G. Vaughan (2015), A ground-based radar for measuring vertical strain rates and time-varying basal melt rates in ice sheets and shelves, *J. Glaciol.*, *61*(230), 1079–1087.

Petra, N., and G. Stadler (2011), Model variational inverse problems governed by partial differential equations, *ICES Tech. Rep. 11–05*, Institute for Computational Engineering and Sciences, Univ. Texas at Austin.

Pettit, E. C., and E. D. Waddington (2003), Ice flow at low deviatoric stress, *J. Glaciol.*, *49*(166), 359–369.

Pettit, E. C., H. P. Jacobson, and E. D. Waddington (2003), Effects of basal sliding on isochrones and flow near an ice divide, *Ann. Glaciol.*, *37*(1), 370–376.

Pettit, E. C., T. Thorsteinsson, H. P. Jacobson, and E. D. Waddington (2007), The role of crystal fabric in flow near an ice divide, *J. Glaciol.*, *53*(181), 277–288.

Raymond, C. F. (1983), Deformation in the vicinity of ice divides, *J. Glaciol.*, *29*(103), 357–373.

Rignot, E., J. Mouginot, and B. Scheuchl (2011), Ice flow of the Antarctic ice sheet, *Science*, *333*, 1427–1430, doi:10.1126/science.1208336.

Rignot, E., J. Mouginot, and B. Scheuchl (2011), Antarctic grounding line mapping from differential satellite radar interferometry, *Geophys. Res. Lett.*, *38*, L10504, doi:10.1029/2011GL047109.

Ross, N., R. G. Bingham, H. F. Corr, F. Ferraccioli, T. A. Jordan, A. Le Brocq, D. M. Rippin, D. Young, D. D. Blankenship, and M. J. Siegert (2012), Steep reverse bed slope at the grounding line of the Weddell Sea Sector in West Antarctica, *Nat. Geosci.*, *5*(6), 393–396.

Scambos, T., J. Bohlander, B. Raup, and T. Haran (2004), Glaciological characteristics of institute ice stream using remote sensing, *Antarct. Sci.*, *16*(02), 205–213.

Siegert, M., N. Ross, H. Corr, J. Kingslake, and R. C. A. Hindmarsh (2013), Late Holocene ice-flow reconfiguration in the Weddell Sea Sector of West Antarctica, *Quat. Sci. Rev.*, *78*, 98–107.

Thoma, M., J. Determann, K. Grosfeld, S. Goeller, and H. H. Hellmer (2015), Future sea-level rise due to projected ocean warming beneath the Filchner Ronne Ice Shelf: A coupled model study, *Earth Planet. Sci. Lett.*, *431*, 217–224.

Vaughan, D., et al. (2013), Observations: Cryosphere, in *Climate Change 2013: The Physical Science Basis. Contribution of Working Group I to the Fifth Assessment Report of the Intergovernmental Panel on Climate Change, book section 4*, pp. 317–382, Cambridge Univ. Press, Cambridge, U. K., and New York, doi:10.1017/CBO9781107415324.012.

Vaughan, D. G., H. F. J. Corr, C. S. M. Doake, and E. D. Waddington (1999), Distortion of isochronous layers in ice revealed by ground-penetrating radar, *Nature*, *398*(6725), 323–326.

Whitehouse, P. L., M. J. Bentley, and A. M. Le Brocq (2012), A deglacial model for Antarctica: Geological constraints and glaciological modelling as a basis for a new model of Antarctic glacial isostatic adjustment, *Quat. Sci. Rev.*, *32*, 1–24.

Winter, K., J. Woodward, N. Ross, S. A. Dunning, R. G. Bingham, H. F. Corr, and M. J. Siegert (2015), Airborne radar evidence for tributary flow switching in institute ice stream, West Antarctica: Implications for ice sheet configuration and dynamics, *J. Geophys. Res. Earth Surf.*, *120*(9), 1611–1625, doi:10.1002/2015JF003518.

Wright, A., and ohters (2014), Sensitivity of the Weddell Sea Sector ice streams to sub-shelf melting and surface accumulation, *Cryosphere*, *8*, 2119–2134.

Zwinger, T., R. Greve, O. Gagliardini, T. Shiraiwa, and M. Lyly (2007), A full Stokes-flow thermo-mechanical model for firn and ice applied to the Gorshkov crater glacier, Kamchatka, *Ann. Glaciol.*, *45*(1), 29–37.